Application of Low-Rank Sparse Decomposition Method to Study Surface Urban Heat Island of Kolkata

Saikat PAUL, SARATH Raj K., B. Bhaskar RAO and Ritu ROY
Department of Architecture & Regional Planning
Indian Institute of Technology, Kharagpur, India

Abstract

In image data analysis Principal Component Analysis (PCA) performs well when the noise is small and Gaussian in nature. However, when the data is non-Gaussian in nature and may contain outliers and spikes, PCA fails. The intrinsic low ranked structure of the datasets can be used to reduce the dimensionality, remove noise and complete missing values by solving a convex Principal Component Analysis (PCA). Surface Urban Heat Island derived from Landsat 8 ETM+ data of Kolkata has been separated into a set of low-rank and sparse components. The Low-rank components depict the linearly correlated data the sparse component represents the perturbation with respect to the mean in the data set. This property is thus useful to assess trends or patterns in the data. Low-rank Sparse Decomposition Method has been used in the field of image processing, bioinformatics, data ranking problems. This study is an attempt to establish RPCA method for studying the trends in Surface Urban Heat Island (SUHI) phenomenon in the metropolitan city of Kolkata.

Key Words: UHI, Low-rank Sparse Decomposition Method, RPCA

1. Introduction

Low rank and sparse decomposition method have been used in data compression and dimension reduction. This study uses the RPCA to assess the evolving pattern of Surface Urban Heat Island for the city of Kolkata. Urban Heat Island (UHI) is a climatic phenomenon which results in an increase of air temperatures in cities compared to the immediate rural areas (Sobstyl et al. 2018; Dos Santos et al. 2017). Surface Urban Heat Island (SUHI) is used to measure the temperature difference between the land surface in rural and urban areas. UHI and SUHI significantly alters the comfort conditions in the urban area thereby increasing the energy requirements for cooling. The land use composition, emissivity and albedo of the surfaces, the storage heat, the energy balance between latent and sensible fractions, and the anthropogenic heat contribute to this phenomenon. This condition is exacerbated by pollution and global climatic perturbations in the form of Climate Change and the ensuing Global Warming. Changes in land surface characteristics of urban areas has also led to increase in the storage heat component in the net energy balance and the temperature within urban areas show hysteresis which is associated with time lag and decrement factor. Energy consumption in different urban processes has led to intensification of SUHI. Peng et al. 2012, studied that vegetation cover assumes a key role in attenuating SUHI in cities thereby mitigating the UHI effect. Several authors have contributed to the research on urban heat Island which has been summarized in table 1.

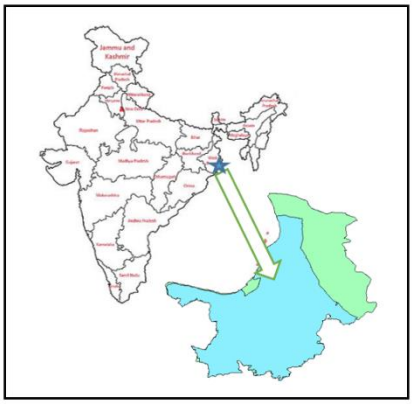

Figure 1: Location map of the study area (Kolkata Metropolitan Area)

Table 1 Factors affecting UHI

S.No.	***Authors***	***Factors affecting UHI in Cities***
1	Peng et al. 2012	Difference in albedo of urban in comparison to rural areas and attenuation effects of vegetation in rural areas
2	Sobstyl et al. 2018	City texture measured by building distribution function and the sky view factor is correlated to UHI
3	Dos Santos et al. 2017	Amplifying effects of developed areas for UHI
4	Menberg et al. 2013	Anthropogenic heat flux contributing to Ground Surface Temperature (GST)
5	Wu et al. 2017	Higher concentration of atmospheric aerosol particles PM2.5 over urban areas reduced UHI intensities by 1◦K attributed to the radiative exchanges by the particles
6	Kumar et al. 2017	Urban rural temperature modulations mainly attributable to moisture availability from irrigation in rural areas and atmospheric aerosols
7	Battaglia et al. 2017	Temperature and RH increase as a result of UHI in urban areas affect semivolatile atmospheric species as nitric acid, ammonia and water affecting the aerosol pH (urban rural aerosol pH differences during intense summer ranging from 0.8 for Baltimore and 0.65 for Chicago)
8	Zhou et al. 2017	Studied the effects of city size and urban form on UHI phenomenon and observed that UHI intensity increased with the logarithm of city size and fractal dimension
9	Ward et al. 2016	Studied Europe wide heat wave and the effects of size of heat island, regional climate and central urban green spaces were found to be significant on Surface Urban Heat Island Magnitude (SUHIM)
10	Martin et al. 2015	Identified the hysteresis effect of global solar radiation (GSR) on surface intra-urban heat islands (SIUHI)
11	Yue and Liu 2016	Green ratio, Plot area, Building density and building height affected the land surface temperature significantly and the urban thermal environment
12	Heaviside et al. 2017	Studied health related risks in urban population compared to rural population due to heat exposure attributable to the UHI effect
13	Zhan et al. 2014	The subsurface urban heat island (SubUHI) intensity reaching first and second extremes in a diurnal temperature cycle lags by about 3.25 and 1.97 hrs per 0.1m

This research explores the daytime variations of Surface Urban Heat Island Intensity (SUHI) in the Kolkata Metropolitan area (figure 1). The correlation of normalised difference vegetation (NDVI) and fractional vegetation cover vis-a-vis the SUHI establish the relationship between the land cover types with the SUHI.

1.1 Low Rank Sparse Decomposition Method

Decomposition of low-rank and sparse components (LRSD) from partial or corrupted measurements is possible for separation of background and dynamic components. LRSD can be used in both static (Hou et al. 2014; Yang et al. 2018; Wen et al. 2016) and dynamic applications (Otazo et al. 2015; Hu et al. 2016; Chen et al. 2015). LRSD method have been used in several application areas including interpreting of MRI scans (Baete et al. 2018; Otazo et al. 2015), to detect voxelwise group differences, CT image sequence restoration (Gou et al. 2013), moving object detection (Hu et al. 2016), face recognition (Hou et al. 2014), discriminating between various sound classes in auditory signals (Lyon et al. 2010) etc.

The LRSD separates the sparse individual variability in the sparse matrix (S) and the essential features in the low rank matrix (L). This method can be applied for studying Surface Urban Heat Island phenomena where input data is temporal in nature and can be separated into background component and sparse component create scenario of deviation from the mean.

2. Methodology

Moderate resolution Landsat 8 ETM+ satellite data has been used for this study. Cloud free satellite data of Kolkata Metropolitan Area was downloaded from the Earthexplorer website for 6th April 2014, 11th April 2016 and 14th April 2017 which corresponds to the summer month having pronounced elevated temperature and clear sky conditions in comparison to other months.

The Landsat data has been corrected for atmospheric attenuations using a dark object subtraction (DOS) method (Nguyen et al. 2015). Dark objects can be assumed to reflect no light, and values greater than zero must result from atmospheric scattering and this is the basis of the DOS method.

The Landsat 8 image Digital Numbers (DNs) were then converted to spectral radiance using appropriate gain and bias values in the image header of the data file, based on equation 1.

$$L = L_{Max} - L_{Min} * 255 * DN + L_{Min} \quad (1)$$

Where,
DN is the degree of greyness of the pixels
L(λ) is radiance in (W/m^2/sr/mm)
L_{Max} and L_{Min} are the calibration constants of the sensor, equal to the maximum and minimum values of the spectral radiance (in W/m^2/sr/mm) detectable for each band, by the sensor Landsat TM.

The noise equivalent delta temperature (NEΔT) of TM/ETM sensors is around 0.2-0.3K. Land Surface Temperature (LST) was calculated from brightness temperature using a single channel method using the band 10 based on the following equations (Jiménez-Muñoz et al. 2014).

$$LST = \gamma[\varepsilon^{-1}(\varphi_1 L_S + \varphi_2) + \varphi_3] + \delta \quad (2)$$

$$\gamma = \left\{\frac{C_2 L_s}{T_b^2}\left[\frac{\lambda^4}{C_1} L_S + \lambda^{-1}\right]\right\}^{-1} \quad (3)$$

$$\delta = -\gamma L_S + T_S \quad (4)$$

where,
L_S = at pixel radiance
T_s = brightness surface temperature
λ = effective wavelength, which was regarded to be 11.5 μm in this research,
ε = surface emissivity,
C1 and C2 = constant values of 1.19104 × 108 μm 4 m^{-2} sr^{-1} and 14387.7 μm K, respectively, and
ϕ_1, ϕ_2, ϕ_3 = atmospheric functions that are calculated using Eqs. (5)–(7) and the amount of water vapor in the atmosphere at the time of imaging.

$$\varphi_1 = 0.14714W^2 - 0.15583W + 1.1234 \quad (5)$$

$$\varphi_2 = -1.1836W^2 - 0.15583W + 1.1234 \quad (6)$$

$$\varphi_3 = -0.04554W^2 - 1.18719W + 0.39071 \quad (7)$$

The SUHI has been derived by differencing the LST with reference to average LST values of rural areas for each dataset.
The satellite images were classified using a maximum likelihood approach in Erdas Imagine Software and classification accuracy was determined by applying Kappa coefficient (Sharma et al. 2015; Li et al. 2011; Shishir & Tsuyuzaki 2018) using the following equation:

$$K = \frac{N\sum_{i=1}^{r} x_{ii} - \sum_{i=1}^{r}(x_{i+} * x_{i+})}{N^2 - \sum_{i=1}^{r}(x_{i+} * x_{i+})} \quad (8)$$

where,
r = number of rows in the error matrix,
xii = number of observations in the ith row and column,
x+i = total number of observations in the ith column, and
N = total number of observations

The fractional vegetation index has been estimated from NDVI using the following linear relationship (Gutman & Ignatov 1998):

$$FVI = \frac{NDVI - NDVI_S}{NDVI_V - NDVI_S} \quad (9)$$

where, $NDVI_S$ and $NDVI_V$ correspond to representative values of NDVI for bare soil (FVC=0) and a vegetation (FVC=1)

$$NDVI = \frac{\rho_{nir} - \rho_{red}}{\rho_{nir} + \rho_{red}} \quad (10)$$

where ρ_{nir} and ρ_{red} are the at-surface reflectivities obtained from sensor bands located in the near infrared (NIR) and red spectral regions of Landsat 8 ETM+.

The mixed pixel emissivity has been determined using an empirical relationship based on an exponential function which is NDVI dependent as proposed by Sobrino et al. 1996.

$$\epsilon_\lambda = \epsilon_{V_\lambda} - (\epsilon_{V_\lambda} - \epsilon_{S_\lambda})\left(\frac{NDVI - NDVI_V}{NDVI_S - NDVI_V}\right)^k \quad (11)$$

where, λ represents the spectral band, ϵ_{V_λ} is the vegetation emissivity (0.99) and ϵ_{S_λ} is the soil emissivity (0.96 Ref. JPL Library Database). $NDVI_V$ is the maximum NDVI for fully vegetated pixel (0.99) and $NDVI_S$ is the minimum NDVI for bare soil (0.15).

Low Rank and Sparse Decomposition (LRSD) is a robust method for separating a rectangular (i,j) matrix **I** into a Low Rank Component (**L**) and a Sparse Component (**S**) :

$$\mathbf{I} = \mathbf{L} + \mathbf{S} \qquad (12)$$

This has been applied on SUHI Images using an inexact augmented Lagrange multiplier method (IALM) (Lin et al. 2011; Erichson et al. 2016) using RRPCA model of RSVD module in R.

3. Results and Discussions

Temporal changes in the extent of vegetation cover has been studied using NDVI for the 3 datasets. Significant changes (improvement in the vegetation content) can be observed in 2016 compared to the 2014 and 2017 when the NDVI values were significantly lower (having lesser vegetation content) due to more intense summer. The implication of this is reflected in the Surface temperature where the increased latent heat fraction results in lowering of the LST on 6th April 2016. The corresponding Fractional Vegetation Index is also high for the 2016 dataset (figure 2).

Emissivity	Land Surface Temperature (°C)	Normalised Difference Vegetation Index (NDVI)	Fractional Vegetation Index	
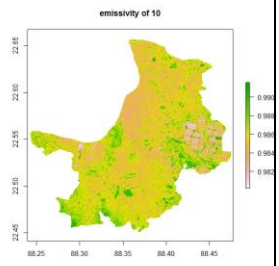	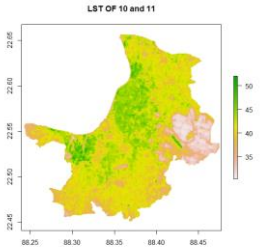	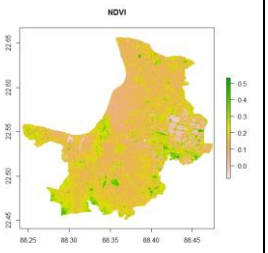	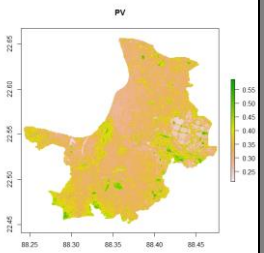	6th April 2014
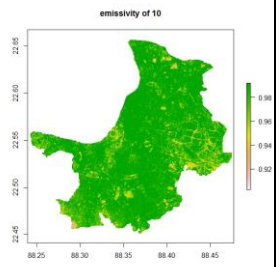	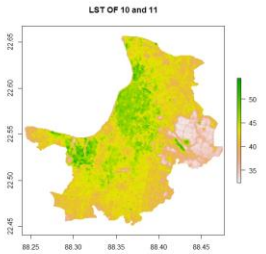	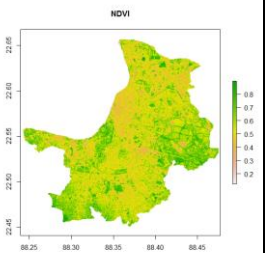	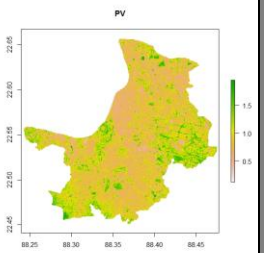	11th April, 2016
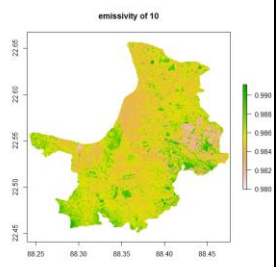	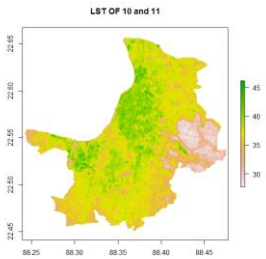	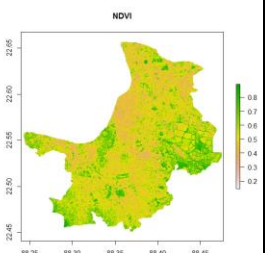	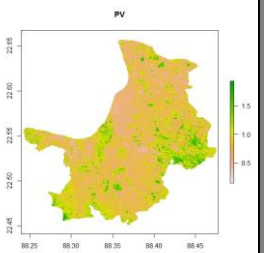	14th April, 2017

Figure 2: Emissivity, LST, NDVI and Fractional Vegetation Index Maps of Kolkata Metropolitan Area

Temporal changes in the extent of vegetation cover has been studied using NDVI for the 3 datasets. Significant changes (improvement in the vegetation content) can be observed in 2016 compared to the 2014 and 2017 when the NDVI values were significantly lower (having lesser vegetation content) due to more intense summer. The implication of this is reflected in the Surface temperature where the increased latent heat fraction results in lowering of the LST on 6th April 2016. The corresponding Fractional Vegetation Index is also high for the 2016 dataset (figure 2).

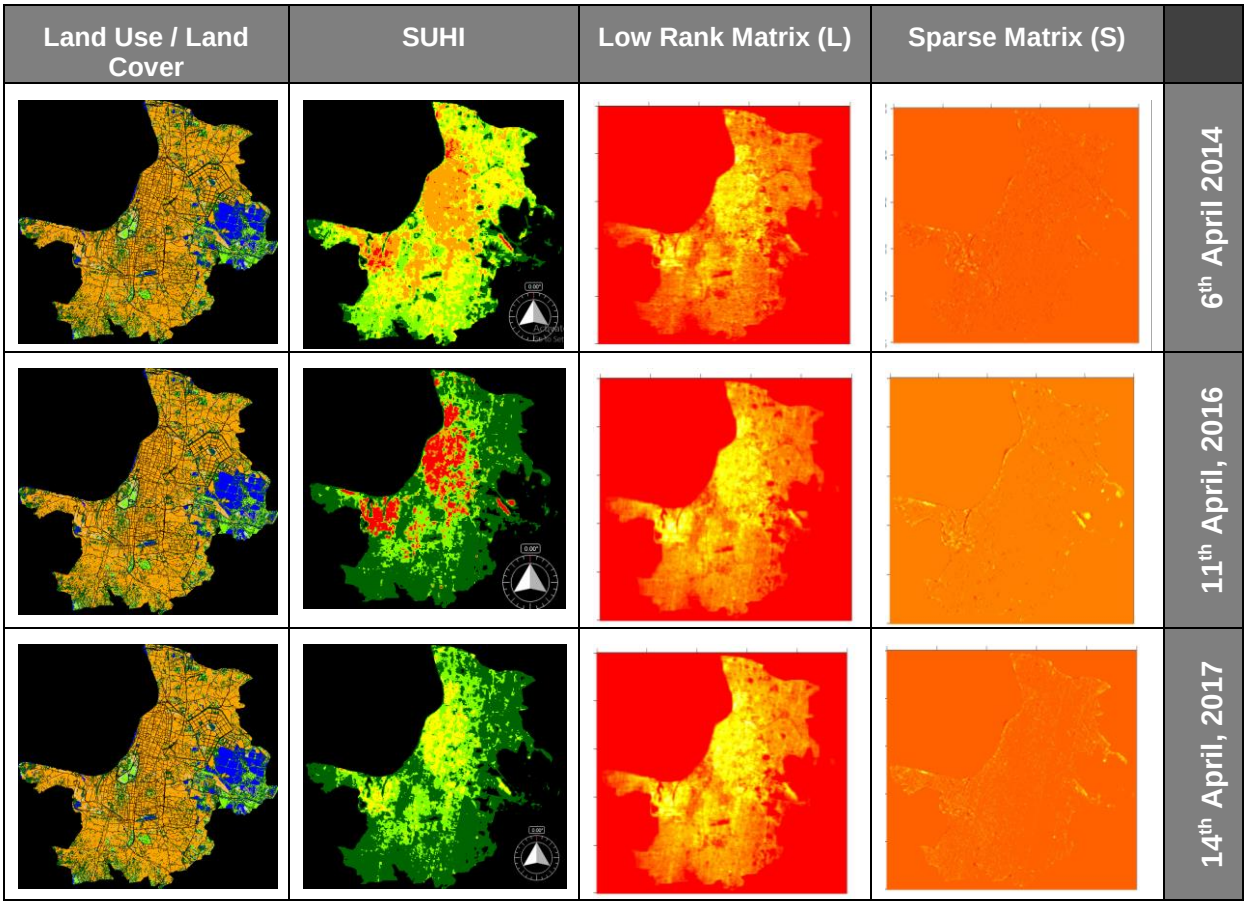

Figure 3: Land Cover, SUHI, Low Rank Matrix and Sparse Matrix of Kolkata Metropolitan Area

4. Conclusion

Low Rank Matrix and Sparse decomposition method can be applied for studying Surface Urban Heat Island (SUHI) phenomena. The temporal data and can be segregated into Low Rank or background component, which depicts commonalities between the time steps and Sparse component, which depicts the dynamic changes in terms of SUHI. The Sparse Component corresponds to changes in SUHI manifested due to changes in either or all parameters of emissivity & albedo which are characteristic of building materials and paved or natural surfaces and built form geometry which signifies re-densification and sprawl or intensification of energy use such as industrial activities or heat emissions due to adoption of cooling or cooling systems.

Thus low rank and sparse decomposition method is a very effective tool to study urban growth and its impact on the s u h i phenomena. this method can be implemented for Big Data Analytics of large volume of satellite derived surface temperature information at a global scale and detect anomalies and device strategies to control and mitigate the effects of these changes.

Acknowledgement:

Landsat-8 image courtesy of the U.S. Geological Survey obtained from earthexplorer.usgs.gov

The authors would like to thank the Ministry of Human Resource Development, Government of India and Indian Institute of Technology Kharagpur for supporting this research.

References:

Baete, S.H. et al., 2018. Low Rank plus Sparse decomposition of ODFs for improved detection of group-level differences and variable correlations in white matter. *Neuroimage*, 174, pp.138–152.

Battaglia, M.A., Douglas, S. & Hennigan, C.J., 2017. Effect of the urban heat island on aerosol ph. *Environmental Science & Technology*, 51(22), pp.13095–13103.

Chander, G., Markham, B.L. and Helder, D.L., 2009. Summary of Current Radiometric Calibration Coefficients for Landsat MSS, TM, ETM+, and EO-1 ALI Sensors. *Remote sensing of Environment*, 113, 893-903.

Chen, S. et al., 2015. Simultaneous Reconstruction and Segmentation of Dynamic PET via Low-Rank and Sparse Matrix Decomposition. *IEEE Transactions on Bio-Medical Engineering*, 62(7), pp.1784–1795.

Dos Santos, A.R. et al., 2017. Spatial and temporal distribution of urban heat islands. *The Science of the Total Environment*, pp.946–956.

Erichson, N. B. , Voronin, S. , Brunton, S., Kutz, J. N. 2016. Randomized matrix decompositions using R. (available at 'arXiv http://arxiv.org/abs/1608.02148)

Gou, S. et al., 2013. CT image sequence restoration based on sparse and low-rank decomposition. *Plos One*, 8(9), pp. 726.

Gutman G., Ignatov A. 1998, The derivation of the green vegetation fraction from NOAA/AVHRR data for use in numerical weather prediction models. *International Journal of Remote Sensing*. 19(8), pp.1533–1543.

Heaviside, C., Macintyre, H. & Vardoulakis, S., 2017. The urban heat island: implications for health in a changing environment. *Current environmental health reports*, 4(3), pp.296–305.

Hou, Y.-F. et al., 2014. Low-rank and eigenface based sparse representation for face recognition. *Plos One*, 9(10), pp.110-118.

Hu, W. et al., 2016. Moving Object Detection Using Tensor Based Low-Rank and Saliently Fused-Sparse Decomposition. *IEEE transactions on image processing : a publication of the IEEE Signal Processing Society*.

J. C. Jiménez-Muñoz, J. A. Sobrino, D. Skoković, C. Mattar, J. Cristóbal, 2014. Land surface temperature retrieval methods from Landsat-8 thermal infrared sensor data, *IEEE Geoscience and Remote Sensing Letters 11* (10), pp. 1840-1843

Kumar, R. et al., 2017. Dominant control of agriculture and irrigation on urban heat island in India. *Scientific reports*, 7(1), pp.140-154.

Li, G. et al., 2011. Land-cover classification in a moist tropical region of Brazil with Landsat TM imagery. *International journal of remote sensing*, 32(23), pp.8207–8230.

Lin, Zhouchen, Liu Risheng, and Su Zhixun, 2011. Linearized Alternating Direction Method with Adaptive Penalty for Low Rank Representation, NIPS 2011. (available at Low rank sparse decomposition remote sensing http://arxiv.org/abs/1109.0367)DOI:10.1016/j.jsb.2012.10.010

Lyon, R.F. et al., 2010. Sound retrieval and ranking using sparse auditory representations. *Neural Computation*, 22(9), pp.2390–2416.

Martin, P., Baudouin, Y. & Gachon, P., 2015. An alternative method to characterize the surface urban heat island. *International Journal of Biometeorology*, 59(7), pp.849–861.

Menberg, K. et al., 2013. Long-term evolution of anthropogenic heat fluxes into a subsurface urban heat island. *Environmental Science & Technology*, 47(17), pp.9747–9755.

Nguyen, H.C. et al., 2015. Optimal Atmospheric Correction for Above-Ground Forest Biomass Estimation with the ETM+ Remote Sensor. *Sensors (Basel, Switzerland)*, 15(8), pp.18865–18886.

Otazo, R., Candès, E. & Sodickson, D.K., 2015. Low-rank plus sparse matrix decomposition for accelerated dynamic MRI with separation of background and dynamic components. *Magnetic Resonance in Medicine*, 73(3), pp.1125–1136.

Peng, S. et al., 2012. Surface urban heat island across 419 global big cities. *Environmental Science & Technology*, 46(2), pp.696–703.

Sharma, R., Chakraborty, A. & Joshi, P.K., 2015. Geospatial quantification and analysis of environmental changes in urbanizing city of Kolkata (India). *Environmental Monitoring and Assessment*, 187(1), pp.420-426.

Shishir, S. & Tsuyuzaki, S., 2018. Hierarchical classification of land use types using multiple vegetation indices to measure the effects of urbanization. *Environmental Monitoring and Assessment*, 190(6), pp.342.

Sobrino, J. A., Z.-L. Li, M. P. Stoll, and F. Becker. 1996. “Multi-Channel and Multi-Angle Algorithms for Estimating Sea and Land Surface Temperature with ATSR Data.” *International Journal of Remote Sensing*, 17 (11), pp. 2089–2114.

Sobstyl, J.M. et al., 2018. Role of city texture in urban heat islands at nighttime. *Physical Review Letters*, 120(10), pp.108.

Ward, K. et al., 2016. Heat waves and urban heat islands in Europe: A review of relevant drivers. *The Science of the Total Environment*, pp.527–539.

Wen, Z., Hou, B. & Jiao, L., 2016. Discriminative Dictionary Learning With Two-Level Low Rank and Group Sparse Decomposition for Image Classification. *IEEE transactions on cybernetics*.

Wu, H. et al., 2017. Urban heat island impacted by fine particles in Nanjing, China. *Scientific reports*, 7(1), pp.11422.

Yang, S., Zhang, K. & Wang, M., 2018. Learning Low-Rank Decomposition for Pan-Sharpening With Spatial-Spectral Offsets. *IEEE transactions on neural networks and learning systems*, 29(8), pp.3647–3657.

Yin, C. et al., 2018. Effects of urban form on the urban heat island effect based on spatial regression model. *The Science of the Total Environment*, 634, pp.696–704.

Yue, W.Z. & Liu, X., 2016. Assessment on heat island effect based on urban regulatory planning. *Ying Yong Sheng Tai Xue Bao = the Journal of Applied Ecology*, 27(11), pp.3631–3640.

Zhan, W. et al., 2014. Satellite-derived subsurface urban heat island. *Environmental Science & Technology*, 48(20), pp.12134–12140.

Zhou, B., Rybski, D. & Kropp, J.P., 2017. The role of city size and urban form in the surface urban heat island. *Scientific reports*, 7(1), pp.4791.